RSC Advances

PAPER

View Article Online
View Journal | View Issue

Published on 11 February 2014. Downloaded by Michigan State University on 29/01/2016 00:21:35.

Cite this: *RSC Adv.*, 2014, **4**, 14822

Learning processes modulated by the interface effects in a Ti/conducting polymer/Ti resistive switching cell†

Fei Zeng,*[a] Sizhao Li,[a] Jing Yang,[a] Feng Pan*[a] and D. Guo[b]

Received 14th November 2013
Accepted 6th February 2014

DOI: 10.1039/c3ra46679e

www.rsc.org/advances

A resistive switching (RS) device of Ti/PEDOT:PSS/Ti, which is favourable for simulating learning processes, was made in this study. The conventional synaptic potentiation, depression plasticity and spike-timing-dependent plasticity, widely studied in neuroscience, were realized in this RS system. Our RS cell can be potentiated under moderate stimulation, but intensive or strong stimulation will trigger the depression mechanism without changing the bias sign. The characterizations of the chemical state suggest that the Ti compound forms at the interface and that PEDOT:PSS contributes to resistance switching and synaptic plasticity. We constructed the energy band diagram for the pristine device to provide a RS cell prototype applied in neuromorphic computing.

Introduction

The requirements for device miniaturization and low power consumption have prompted researchers to find intelligent computing modes and circuits. The simulation of neuromorphic networks is a popular topic in the field of novel computer and related materials. Mimicking neural synaptic plasticity by using memristors has attracted considerable interest from scientists because a memristor with a simple sandwich or field effect transistor structure may replace a set of complex circuits to realize basic learning functions.[1–10] People have tried to simulate conventional synaptic potentiation and depression plasticity in many memristor systems, as well as the widely studied spike-time-dependent plasticity (STDP) in neuromorphic computation.[8,11,12] However, the type of system that can be applied in the future is still unclear. Scientists that major in neuromorphic computing have also entered into this interdisciplinary field. They have evaluated some typical memristors by computer simulation and have stated that considerable studies need to be conducted to achieve a memristor that acts as an independent artificial synapse.[13,14] Two typical problems have been proposed for memristors that are integrated in a crossbar configuration. First, the resistivity of the low resistance state needs to be enhanced because the power consumption of the crossbar array will be high.[13] Second, the memory node with low resistance will be activated to suppress other memory nodes in the crossbar arrays, thus leading to system instability.[14]

Our group has tried to mimic synaptic plasticity by modulating the state of the organic/inorganic interface in conducting polymer-based memristors.[15] We propose a resistive switching (RS) cell wherein the naturally formed oxide layer increases the memristor resistance. This structure may be used to reduce power consumption in neuromorphic circuits. In this paper, we use poly(3,4-ethylenedioxythiophene):poly(styrenesulfonate) (PEDOT:PSS) as the interlayer of the sandwiched RS cell but change the electrode to Ti. The new RS cell displays current–voltage properties that are quite different from the typical ohm properties, resistance switching, or negative differential resistance (NDR). The conductance of the RS cell is enhanced systematically under consecutive stimulations with moderate strength. However, a NDR is found under high strength stimulations if the input direction is unchanged. Such a property is suitable for simulating learning processes. We have successfully mimicked the conventional synaptic potentiation, depression plasticity and STDP. The possible mechanisms of the proposed RS cell are related to the RS of the interfacial layer (*i.e.*, the naturally formed Ti compound) and the de-doping of the PEDOT:PSS. Two types of RS have contrasting bias with the same sign. The activation thresholds of the two types of RS are low (~−1 V) and high (~−2.5 V). An energy band diagram was proposed for the pristine device. Our RS cell may enhance stability when it is integrated into crossbar arrays and acts as an artificial synapse in neuromorphic computing.

Experimental details

A PEDOT:PSS water-based solution was purchased from Sigma-Aldrich Co. Ltd. and used as supplied. The PEDOT and PSS

[a]*Key Laboratory of Advanced Materials (MOE), School of Materials Science & Engineering, Tsinghua University, Beijing 100084, China. E-mail: zengfei@mail.tsinghua.edu.cn; panf@mail.tsinghua.edu.cn; Fax: +86-10-62771160; Tel: +86-10-62795373*

[b]*Institute of Acoustic, Chinese Academy of Science, China*

† Electronic supplementary information (ESI) available. See DOI: 10.1039/c3ra46679e

This journal is © The Royal Society of Chemistry 2014

Published on 11 February 2014. Downloaded by Michigan State University on 29/01/2016 00:21:35.

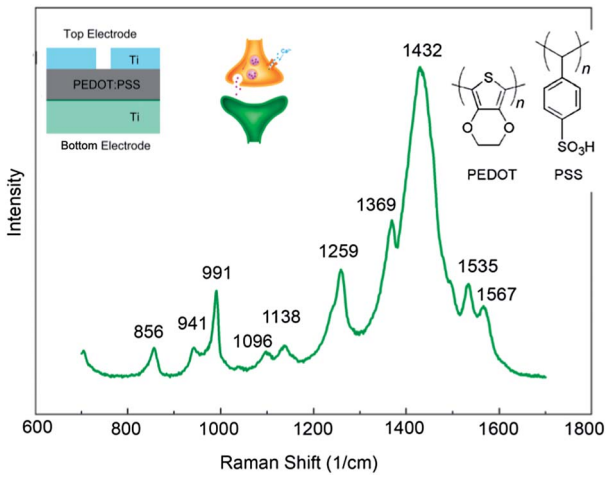

Fig. 1 Schematic of the memory cell with Si/Ti/PEDOT:PSS/Ti junctions, the chemical structures of PEDOT and PSS and the Raman spectrum of PEDOT:PSS.

contents are 0.5% and 0.8% w/w, respectively. Fig. 1 shows the structure of the device, the chemical structures of PEDOT and PSS and the Raman spectrum of the PEDOT:PSS. The Ti/PEDOT:PSS/Ti junctions were composed of a Ti top electrode (TE) and a Ti bottom electrode (BE) with a thickness of approximately 50 nm. Both the TE and BE were prepared by electron beam vaporisation. The TEs were deposited through shadow masks with diameters of 300 μm. The layer of PEDOT:PSS was spin coated onto the BE and baked on a hot plate at 120 °C for 20 min in a nitrogen-filled glove box (O_2, H_2O < 1 ppm). Before spin coating, the aqueous PEDOT:PSS solution was filtered through a micro filter membrane with a pore size of 0.45 μm. The filtered PEDOT:PSS solution was spin coated onto the Si/Ti substrate at 500 rpm for 10 s, at 3000 to 5000 rpm for 30 s and at 1500 rpm for 20 s. The thickness of the individual layer was calibrated by using a surface profiler (Veeco Dektak 150). The thicknesses of the PEDOT:PSS layers were 100, 85, 70 and 55 nm.

Electrical characterizations were performed on an Agilent B1500A semiconductor device analyser (Agilent, USA) under ambient conditions without any encapsulation. Voltages were applied to the TE, and the BE was grounded for all measurements. During the electrical measurements, the RS cells were placed on a Cascade M150 measurement platform. The chemical states of interfaces were analysed by using Ti $L_{2,3}$ edge X-ray absorption near edge spectroscopy (XANES), which was performed in the BL08U station of the Shanghai Synchrotron Radiation Facility. Cross-sectional transmit high resolution electron microscopy (HRTEM) images were used to examine interface states.

Results and discussion

1. Basic electrical characteristics

Fig. 2 shows the electrical characteristics of the Ti/PEDOT:PSS/Ti junctions measured between ±3.0 V. The current–voltage (*I–V*) curves vary with scanning number and have a complicated nonlinearity feature and are not influenced qualitatively by the film thickness (Fig. S1†). An *I–V* loop is formed upon the completion of every voltage scan at ±3.0 V. The loops decrease with the scanning number, *i.e.*, the variation trend from the 1st scan to the 20th scan. The *I–V* curve obtained after the 1st scan is different from the *I–V* curve in the last scan. The pristine device is in a high resistance state (Fig. 3(a)). The current (or the conduction) increases quickly after the negative bias exceeds −1 V and varies slowly after −2 V. Moreover, the NDR behaviour appears around −2.5 V. The conduction is higher during the scan from 3 V to 0 V than from 0 V to 3 V when the sign of the bias is reversed (processes 3 and 4 in Fig. 3(a)). The pattern of the *I–V* curve in the 2nd scan resembles the pattern of the *I–V* curve in the 6th scan (Fig. 3(b)), which has the features of typical non-volatile memory curves.[16–18] Process 3 crosses over with process 4 in the 7th scan to the 10th scan (Fig. 3(c)). The dynamic NDR behaviour dominates in both the 1st and 2nd quadrant from the 11th voltage scan (Fig. 3(d)). Our device is different from the conventional linear resistor, negative differential resistor and typical RS memory.[16–19] Two RS mechanisms should work during the voltage scan in Fig. 3, specifically in Fig. 3(a). One mechanism has a threshold of around −1 V (Fig. 3(a)), whereas the other mechanism has a threshold larger than 2 V.

2. Simulating synaptic plasticity

The current (or conduction) variation shown in Fig. 2 and 3 is favourable for simulating learning processes and synaptic plasticity if the former is compared with the latter. According to

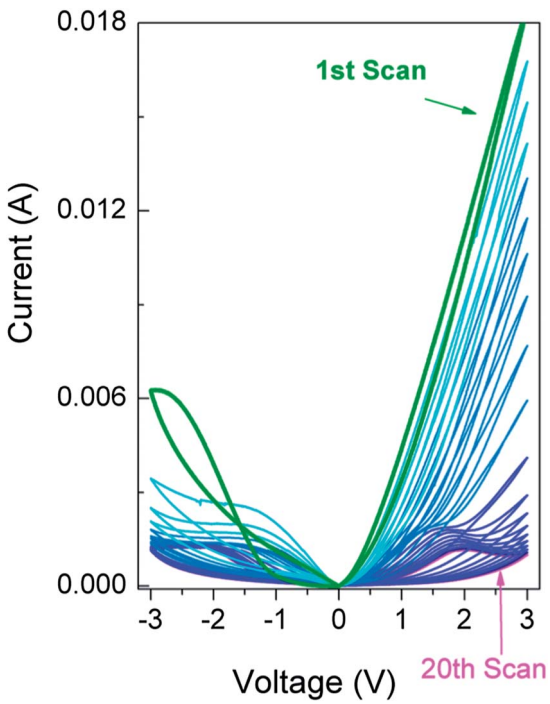

Fig. 2 Current–voltage (*I–V*) properties of Ti/PEDOT:PSS/Ti junctions obtained from 20 scans between ±3 V. 1st scan: bold green line, 20th scan: pink line.

Published on 11 February 2014. Downloaded by Michigan State University on 29/01/2016 00:21:35.

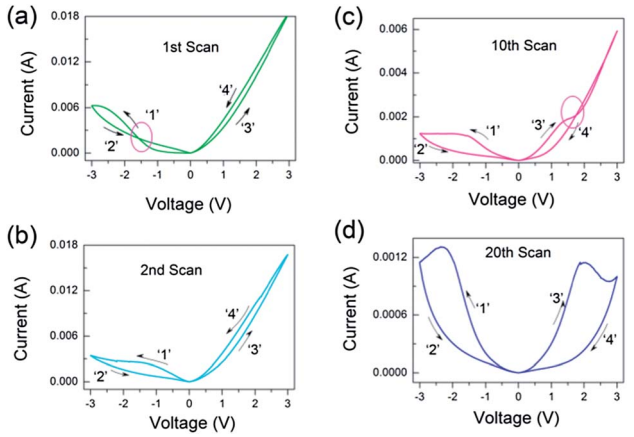

Fig. 3 The *I*–*V* properties of (a) 1st, (b) 2nd, (c) 10th, and (d) 20th scans in Fig. 2. Two red ovals indicate crossovers in the 1st and 10th scans. The scanning direction follows the number and direction of the arrows on each scan.

neuroscience and physiology, the synaptic weight sharply increases to a certain extent when the stimuli value is higher than the threshold value. Excess stimulation will depress the synaptic weight to prevent system collapse.[20] Our pristine device should be triggered to a high conductive state (HCS) by using consecutive moderate inputs, but should be depressed from the HCS after consecutive strong inputs (Fig. 2 and 3). Considering the above analogies, we simulated the synaptic plasticity by using our device.

First, the input with the largest absolute value of 1 V was used to test the plasticity under moderate inputs. Fig. 4(a) shows the response to consecutive DC scans as well as those done in the literature.[2,21] Fig. 4(b) shows that the rectangle wave is used as the action potential (AP) and the current variation can be simply treated as the synaptic weight. It is potentiated under consecutive stimulation with a negative sign but is depressed under a reversed bias sign (Fig. 4(b)). The synaptic behaviour in the range of ±1 V resembles the synaptic behaviour of a Ag/PEDOT:PSS/Ta RS cell in the range of ±2 V.[15]

Second, varied pulse heights were used to examine modifications of the synaptic behaviour of the RS cell.[10,22] The form of the stimulations was reorganized to a system in which a set of −1 V inputs were followed by a set of −3 V inputs. The response to the DC scan was also checked in Fig. 5(a) before the pulse input was used. The conductance increases first with −1 V inputs (Fig. 5(a)). However, when the inputs are changed to −3 V, the absolute value of the conductance or synaptic weight is enhanced intensively but cannot be maintained at such a high value in the following stimulations. On the contrary, the conductance decreases subsequently with the input number even if the pulse height was reduced subsequently. This is consistent with the NDR effect observed in Fig. 2 and 3. It corresponds to a physiological behaviour wherein depression occurs after intensively strong stimulations.[20,23,24] This behaviour is considered long-term depression in neuroscience and is an important learning mechanism that is related to habit and adaptation. We know that our RS cell displays plasticity close to that of the biological synapse. Our RS cell can be potentiated and depressed under stimulations with the same signs but different threshold values (Fig. 4 and 5). The required thresholds for the potentiation and depressed plasticity are moderate and high, respectively. We then used the pulses of −1 V and the followed pulses of −3 V. One can see easily the potentiation under the pulse under −1 V. However, the pulse of −3 V enhanced the conduction quickly but decreased the conduction subsequently (Fig. 5(b)).

A recent study has shown that a memristor with low resistance will be potentiated preferably and maintain this advantage subsequently.[14] This situation does not benefit the stability of the crossbar configuration. The activated memristor will cause a system collapse while the other memristors are still dormant. Subsidiary circuits, such as compliance current circuits, are required to solve this "bottleneck",[14] thus increasing the complications and difficulties in manufacturing and control. However, these complications and difficulties may be solved by using device like ours owing NDR effects,[25,26] in contrast to adding other circuits or by changing the sandwiched structure.

In the previously published works aiming to mimic synaptic plasticity, rectangle pulses were generally used to simulate potentiation or depression in one bias direction.[1–4,10,15,21] Some even used pulses with different heights. Though these are easily realized in electronics, we should know that all synaptic plasticity induction protocols are based on identical action potentials (APs). Thus, it is useful and meaningful to use identical APs. Summarizing the results in Fig. 4 and 5, we think that it is meaningful to use pulses with an unchanged height of 1 V to mimic the simple Hebbian learning rule (shown in Fig. 4(b)). However, care is needed to use results in Fig. 5, though they suggest metaplasticity of our device.[27] Their exact relationships in physiology or biology need to be clarified.

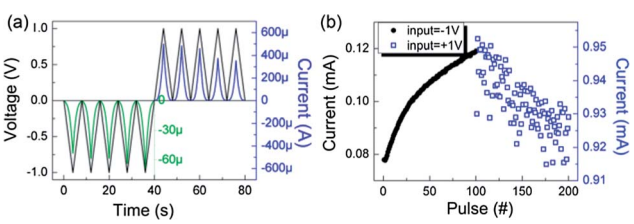

Fig. 4 (a) The responses to five DC scans in (0, −1 V) + 5 scans in (0, +1 V); (b) simulating synaptic plasticity with moderate inputs. Potentiation in 100 pulses of −1 V + depression in 100 pulses of +1 V.

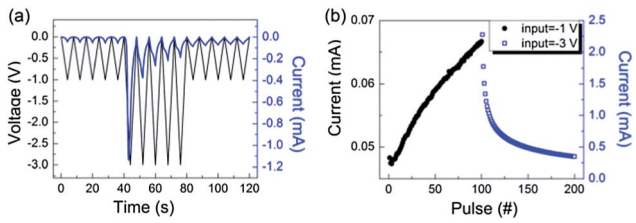

Fig. 5 (a) The responses to five DC scans in (0, −1 V) + 5 scans in (0, −3 V) + 5 re-scans in (0, −1 V); (b) synaptic plasticity modified by strong inputs. Potentiation in 100 pulses of −1 V + depression in 100 pulses of −3 V.

This journal is © The Royal Society of Chemistry 2014

Published on 11 February 2014. Downloaded by Michigan State University on 29/01/2016 00:21:35.

If our device structure would be used to solve the memristor competing problem,[14] it should realize STDP. STDP, which is based on the Hebbian learning rule, is a widely studied learning model in neuroscience.[8,11,12] STDP denotes that the synaptic weight can be modified by the precise timing between pre- and post-synaptic spikes. If a post-synapse is stimulated momentarily after a pre-synapse, the synaptic weight increases and long-term potentiation occurs; if the order of the pairing is reversed, the synaptic weight decreases and long-term depression occurs. Thus, STDP has been simulated by research groups to examine its potential in neuromorphic computing for memory devices.[2,3,7,10,15,21]

We then tested the STDP protocol in Fig. 6 based on the above considerations. Since real APs involve ion migration through a membrane, a pulse with a fixed sign is inappropriate. Previous works have adopted a pulse form analogous to the real AP when the external neuron circuit is absent.[5,15,21,28] Various AP forms were presented and their effects on the patterns of plasticity were discussed.[13] We selected one AP form (spike pair) enumerated in ref. 13 for convenience and plotted it in Fig. 6(a). The TE and BE were defined as the pre- and post-synapse, respectively.

Fig. 6 shows the simulation results using our RS cell. The synaptic weight varies with the relative spike timing (δt). The synaptic weight was defined as $(I_2 - I_1)/I_1$. The post-synaptic currents were measured before (I_1) and 7 min after (I_2) the spike pair was applied. The STDP pattern resembles the reported STDP in biology synapses. The synaptic weight is at its highest value when the pre- and post-spikes nearly overlap with each other, *i.e.*, δt is around zero (Fig. 6(a)). When the pre-synaptic spike is triggered before the post-synaptic spike, *i.e.*, $\delta t < 0$, the synaptic weight is high and corresponds to the potentiation effect; otherwise, *i.e.*, $\delta t > 0$, the synaptic weight is lower and corresponds to the depression effect. The synaptic weights can be fitted by using the following equation:

$$\Delta W = w_0 + A \exp(-\delta t/t) \quad (1)$$

For $\delta t < 0$, $A^+ = 0.8398$, $\tau^+ = 16.9$ ms and $w_0 = 0.54$; for $\delta t > 0$, $A^- = 0.32$, $\tau^- = 12.7$ ms and $w_0 = 0.45$. Different from other works,[2,21] we did not obtain $w_0 = 0$ in Fig. 6(b) because of the strong stimulation with a value of −3 V to enhance the conductance to a high level (Fig. 2 and 3(a)). The results in Fig. 6(b) confirm in principle the possibility of our device being used in neuromorphic computing.

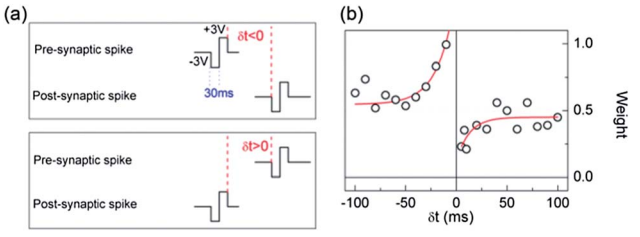

Fig. 6 Simulating STDP. (a) Spike pairs used for measurement. The TE and BE were defined as the pre- and post-synapse, respectively. (b) The variation trend of synaptic weight, defined as $(I_2 - I_1)/I_1$, with the relative spike timing (δt). The post-synaptic currents were measured before (I_1) and 7 min after (I_2) the spike pair application. The amplitude of the read voltage was 0.1 V.

3. Mechanisms of electrical characteristics and synaptic plasticity

To understand the mechanism of our RS cell, XANES spectra and cross-sectional TEM images were used to examine the interface states between the electrode and the conducting polymer. Fig. 7 shows the XANES spectra of the Ti electrodes at the $L_{2,3}$ edge. The spectrum of the Ti BE was obtained after the coated PEDOT:PSS was removed, whereas the Ti TE used for the XANES measurement was 2.5 nm, which was thin enough for the penetration by synchronized X-ray. By referring to the typical spectra of the Ti $L_{2,3}$ edge in the form of metal, oxide and sulphide compounds,[29–31] changes that occur at the interface can be concluded. For the Ti BE, the strengths of the Ti $L_{2,3}$ edge and ratios of the L_2 to L_3 edge are weaker than the strengths and ratios of the pure Ti film without any polymer deposited on it. Obviously, the surface of the Ti BE is oxidized to some extent. The XANES of the Ti TE vary little compared with the XANES of the pure Ti film, thus indicating that the pristine Ti TE is only weakly oxidized at the Ti TE/polymer interface. The interfaces at the TE and BE are initially asymmetrical, although the nominal device structure is symmetrical. This situation occurred because of the preparation process wherein baking is required after the PEDOT:PSS is spin coated.

In the XANES spectroscopy of the Ti BE, there is hardly any peak shift of 459.4 and 464.9 eV, indicating that the signal of metallic Ti electrode is strong and that the interface compound is very thin. However, the peaks of 457.6 and 463 eV are increased and the peaks of 459.4 and 464.9 were broadened greatly. The ratios of I (457.9 eV)/I (459.4 eV) and I (463 eV)/I (464.9 eV) are enhanced significantly. These results suggest the formation of TiS_3 according to ref. 31. However, TiO_x and Ti oxysulfide cannot be excluded in these spectra. Additionally, we found that the interface layer is amorphous initially (Fig. 8(a)) and the crystalline structure could not be determined. Therefore, we refer to the formation of the Ti compound instead of either single TiS_x or TiO_x at the interface on the Ti BE.

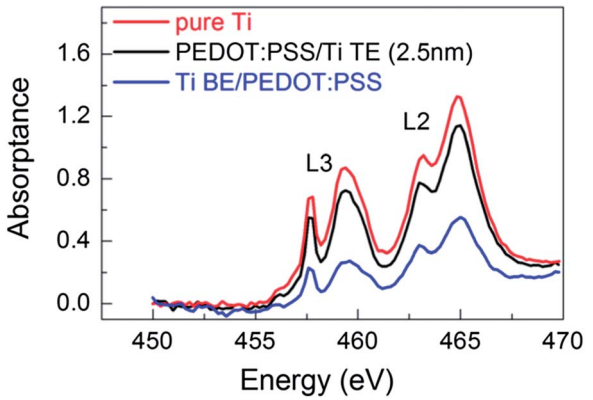

Fig. 7 Ti $L_{2,3}$ edge XANES spectra obtained before electrical manipulation.

Published on 11 February 2014. Downloaded by Michigan State University on 29/01/2016 00:21:35.

Fig. 8(a) and (b) shows the cross-sectional HRTEM images of a pristine device obtained near the BE and TE, respectively. One can clearly see the interface layers existing between the electrodes and the polymer layer according to the contrast in the HRTEM images. The interface layer is not quite homogenous for the pristine device due to the initial interface roughness. However, the roughness was improved after the device was electrically manipulated. We read the interface thickness from the local positions labelled in Fig. 8. The transition can be observed from crystalline structures to an amorphous interface and amorphous polymer layer in the zoomed-in HRTEM images about the interface (shown in Fig. S2 & S3†). The thickness near the BE is around 5.0 nm and that near the TE around 4.5 nm, which is consistent with the XANES spectra. Since PEDOT:PSS is a p-type semiconductor, the naturally oxidised Ti compound should be an n-type semiconductor according to the initial rectified *I–V* curves shown in Fig. 2 and 3.

Consequently, the energy band diagram is plotted for the pristine device in Fig. 9 on the basis of the above structural analysis. The Ti compound at the BE interface is the initial origin of the high resistance and should be an n-type semiconductor to form a p–n junction with PEDOT:PSS. The Ti compound will be switched under the loaded negative bias and changed to low resistance, thus resembling the behaviour of the TO_x memristor. The RS of the Ti compound can be confirmed as discussed in the following sections, but its real mechanism is still under debate. The rapid increase in the current (Fig. 3(a)) will induce PEDOT:PSS de-doping and PSS accumulation at the interface (indicated by the dashed line in Fig. 9),[32] thus leading to the NDR behaviour and conductance decrease.

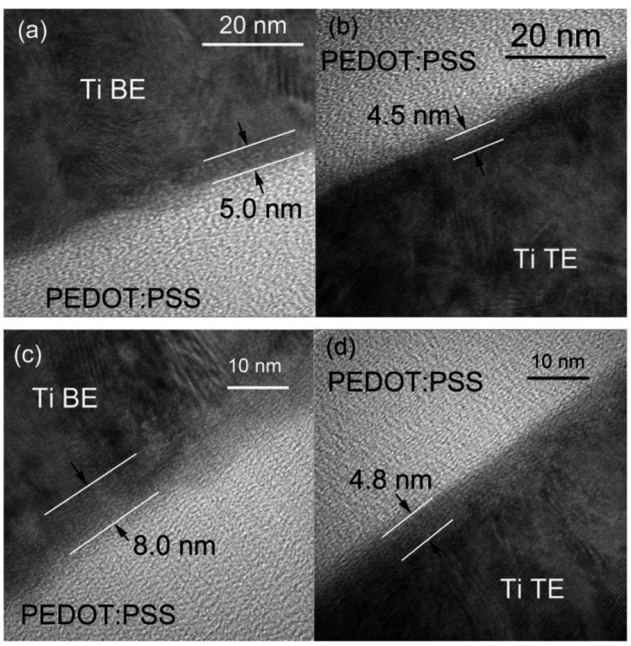

Fig. 8 Cross-sectional HRTEM images of the interfaces obtained at (a) Ti BE/PEDOT:PSS and (b) PEDOT:PSS/Ti TE for the pristine device. The interfaces at (c) the Ti BE/PEDOT:PSS and (d) PEDOT:PSS/the Ti TE for the device with the NDR behaviors appeared in both the first and the second quadrants (as shown in Fig. 3d).

Considering *I–V* curves are vary with scanning number in Fig. 2 and 3, we tested the device stability. It has been found from Fig. 2 and 3 that the devices are easily modified by strong electric fields. However, they are stable in weak electric fields, *e.g.*, the ±0.5 V scans in Fig. S4(a).† Thus, the electrical characteristics after strong stimulation were tested using ±0.5 V scans (Fig. S5†). It is seen that the 5 consecutive scans using ±0.5 V are nearly superposed after 5 scans at ±2.0 V, while there is very low divergence from each other after 5 scans at ±3.0 V. This result demonstrates that even if the state of the device is modified by a strong stimulation, the modified state could be conserved under a load of low magnitude.

The polarity of the RS activated at around −1 V was tested by loading −1 V over five consecutive times and reverse loading to +1 V for the following five times. The absolute value of the current was found to rise step by step in the five consecutive loadings of −1 V but to descend sequentially in the five consecutive loadings of +1 V (indicated using black arrows in Fig. 10(a)), which is consistent with Fig. 4(a). This demonstrates that the RS activated at around −1 V is bipolar, in which the potentiation of the current (or conductivity) is driven by negative bias, while the depression of the current (or conductivity) is prompted by positive bias. Thus, the RS activated at around −1 V is assumed to relate to the Ti compounds which may form between the BE and the polymer due to the baking process. Its RS property is similar to many TiO_x-based bipolar memory devices. The migration of oxygen ions may account for the RS of the Ti compound. However, the properties of the Ti compounds should be modulated by the neighboring polymer as observed in the multi-layer structure of the Ti (or TiO_x) compound. Fig. 10(b) suggests the existence of such modulation. If the consecutive bias of −1.5 V is loaded, an *I–V* loop could be observed in the first scan. The current (or conductivity) rises in the first scan but descends slightly in the following four scans (indicated by black arrows), which implies that some depression mechanism is triggered by the rapid rise in current.

To understand the origin of this depression mechanism, we exchanged both the TE and BE for Au electrodes, and obtained the *I–V* results shown in Fig. 10(c). Evidently, symmetrical dynamic NDR behaviors are present in Fig. 10(c). The points of inflection for the dynamic NDR are around 2 to 2.5 V. The *I–V* properties are non-polar and volatile. The *I–V* curve is linear under low bias, the initial conductivity being much higher than in our Ti/PEDOT:PSS/Ti junctions. No rapid, RS-induced rise in

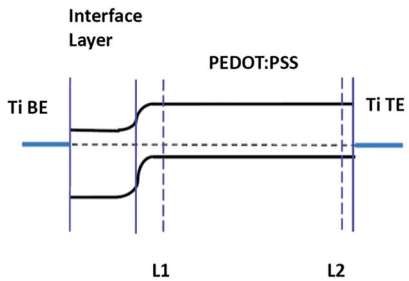

Fig. 9 Energy band diagram of the pristine device.

 This journal is © The Royal Society of Chemistry 2014

Published on 11 February 2014. Downloaded by Michigan State University on 29/01/2016 00:21:35.

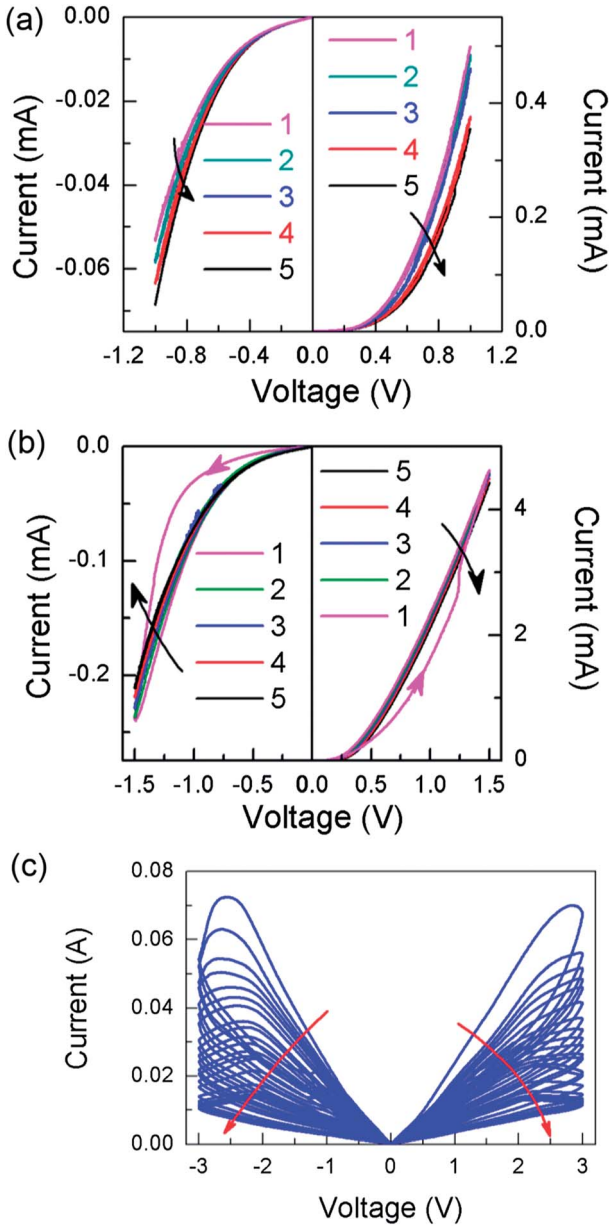

Fig. 10 *I–V* curves comparison between Ti/PEDOT:PSS/Ti and Au/PEDOT:PSS/Au junctions. (a) *I–V* curves of the Ti/PEDOT:PSS/Ti junctions obtained under consecutive direct current (DC) scans. Left: five scans in (0, −1 V). Right: five scans in (0, +1 V). (b) *I–V* curves of the Ti/PEDOT:PSS/Ti cells obtained under DC scans. Left: five scans in (0, −1.5 V). Right: five scans in (0, +1.5 V). (c) *I–V* curves of Au/PEDOT:PSS/Au junction obtained after 20 scans between ±3 V.

current was observed for the Au/PEDOT:PSS/Au junctions. Some studies have pointed out that the differences in the hole injection efficiencies of the two electrodes will lead to de-doping of the $PEDOT^+$ and reduction of current (or conductivity) if the electrical field is raised to some value.[32,33] Thus, we believe that the dynamic NDR in Fig. 2 and 3 comes from the de-doping of the $PEDOT^+$, which could be written as

$$PEDOT^+ + e^- = PEDOT^0 \quad (2a)$$

$$PSS^- - e^- = PSS \quad (2b)$$

This process is charge balanced in PEDOT:PSS. The asymmetric interface between the BE and TE strengthens the difference of the hole injection efficiency and results in depression effects in Fig. 10(b) under lower values of bias.

The structure change of PEDOT:PSS would lead to separation of PEDOT and PSS, and accumulation of PSS near the electrodes.[32] The Ti compound layer would grow during this process. Fig. 8(c) and (d) show cross-sectional TEM images of the interfaces at the Ti BE/PEDOT:PSS and PEDOT:PSS/Ti TE interfaces, respectively, for a device with NDR behaviours appearing in both the first and second quadrants (as shown in Fig. 2(e)). The interface boundaries are less well-defined than those shown in Fig. 8(a) and (b). The estimated thickness of the interface near the Ti BE is about 8.0 nm and that near the Ti TE is about 4.8 nm. The thickened interfaces might have arisen as a consequence of the diffusion of oxygen, the adsorption of PSS, or a combination of the two. The elementary distributions across the junction were examined using EDX in TEM as shown in Fig. S6.† The profile of the Ti counts illustrate that the Ti content is flat and negligible in the middle of the polymer layer, indicating that the Ti element did not diffuse deeply into the polymer. The oxygen counts are high in both interfaces near the BE and TE. The peak of the sulphur counts is slightly outside the peak of the oxygen counts around the interface from the BE. This accumulation of sulphur near the electrodes is related to both preparation and subsequent electrical manipulation. The carbon counts are lower in both interface layers near the BE and the TE.

The above results suggest that the interface may be dynamically moved after the strong consecutive stimulations. The *I–V* properties of our RS cell may resemble unipolar RS. There are two types of the unipolar RS. One occurs normally depending on the connection and fusing of one type of conducting filament. The voltage of fusing, *i.e.*, RESET voltage, is usually lower than the voltage turning from the low resistance state to the high resistance state, *i.e.*, SET voltage.[34] Another is the memory structure also owing the NDR effect, such as that of a SiO_x-based RS cell.[25,26] We suggest that the latter is suitable for mimicking synaptic plasticity according to this study. Our RS cell might provide a prototype for the crossbar configuration.

Conclusions

We have fabricated a RS structure of Ti/PEDOT:PSS/Ti that is favourable for simulating learning processes. On the basis of the understanding of the DC *I–V* properties, we have mimicked conventional synaptic potentiation, depression plasticity and STDP. Our RS cell can be potentiated under moderate stimulations, but intensive or strong stimulations will trigger the depression mechanism without changing the bias sign. These properties may provide stability while integrating the memristor into the crossbar configuration. The characterizations of the chemical state demonstrate that the Ti compound formed at the interface and PEDOT:PSS contributes to the RS; the thresholds of the former and latter are low and high, respectively. We constructed the energy band diagram for the pristine

Published on 11 February 2014. Downloaded by Michigan State University on 29/01/2016 00:21:35.

device to provide a reference for applying the RS cell on neuromorphic computing.

Acknowledgements

This work was supported by National Natural Science foundation of China (Grant no. 51371103 and 51231004), National Basic Research Program of China (Grant no. 2010CB832905) and National Hi-tech (R & D) project of China (Grant no. 2012AA03A706, 2013AA030801 and SS2014AA032604), the Research Project of Chinese Ministry of Education (no. 113007A), Hundred Talents Program' of Chinese Academy of Sciences.

Notes and references

1 T. Ohno, T. Hasegawa, T. Tsuruoka, K. Terabe, J. K. Gimzewski and M. Aono, *Nat. Mater.*, 2011, **10**, 591–595.
2 S. H. Jo, T. Chang, I. Ebong, B. B. Bhadviya, P. Mazumder and W. Lu, *Nano Lett.*, 2010, **10**, 1297–1301.
3 D. Kuzum, R. G. D. Jeyasingh, B. Lee and H. S. P. Wong, *Nano Lett.*, 2012, **12**, 2179–2186.
4 T. Chang, S. H. Jo and W. Lu, *ACS Nano*, 2011, **5**, 7669–7676.
5 F. Alibart, S. Pleutin, D. Guérin, C. Novembre, S. Lenfant, K. Lmimouni, C. Gamrat and D. Vuillaume, *Adv. Funct. Mater.*, 2010, **20**, 330–337.
6 V. Erokhin, T. Berzina, K. Gorshkov, P. Camorani, A. Pucci, L. Ricci, G. Ruggeri, R. Sigalad and A. Schüzd, *J. Mater. Chem.*, 2012, **22**, 22881.
7 Q. X. Lai, L. Zhang, Z. Y. Li, W. F. Stickle, R. S. Williams and Y. Chen, *Adv. Mater.*, 2010, **22**, 2448–2453.
8 G. Rachmuth, H. Z. Shouval, M. F. Bear and C. S. Poon, *PNAS*, 2011, **108**, E1266–E1274.
9 D. S. Jeong, I. Kim, M. Ziegler and H. Kohlstedt, *RSC Adv.*, 2013, **3**, 3169–3183.
10 Y. Li, Y. P. Zhong, L. Xu, J. J. Zhang, X. H. Xu, H. J. Sun and X. S. Miao, *Sci. Rep.*, 2013, **3**, 1619.
11 S. Song, K. D. Miller and L. F. Abbott, *Nat. Neurosci.*, 2000, **3**, 919–926.
12 G. Q. Bi and M. M. Poo, *J. Neurosci.*, 1998, **15**, 10464–10472.
13 C. Zamarreño-Ramos, L. A. Camuñas-Mesa, J. A. Pérez-Carrasco, T. Timothée Masquelier, T. Serrano-Gotarredona and B. Linares-Barranco, *Front. Neurosci.*, 2011, **5**, 26.
14 F. M. Bayat, S. B. Shouraki and I. E. P. Afrakoti, *Neurocomputing*, 2013, **115**, 166–168.
15 S. Z. Li, F. Zeng, C. Chen, H. Liu, G. S. Tang, S. Gao, C. Song, Y. S. Lin, F. Pan and D. Guo, *J. Mater. Chem. C*, 2013, **1**, 5292–5298.
16 K. M. Kim, B. J. Choi, M. H. Lee, G. H. Kim, S. J. Song, J. Y. Seok, J. H. Yoon, S. Han and C. S. Hwang, *Nanotechnology*, 2011, **22**, 254010.
17 J. J. Yang, F. Miao, M. D. Pickett, D. A. A. Ohlberg, D. R. Stewart, C. N. Lau and R. S. Williams, *Nanotechnology*, 2009, **20**, 215201.
18 D. H. Kwon, K. M. Kim, J. H. Jang, J. M. Jeon, M. H. Lee, G. H. Kim, X. S. Li, G. S. Park, B. Lee, S. Han, M. Y. Kim and C. S. Hwang, *Nat. Nanotechnol.*, 2010, **5**, 148–153.
19 D. B. Strukov, G. S. Snider, D. R. Stewart and R. S. Williams, *Nature*, 2008, **453**, 80–83.
20 M. E. Bear, B. W. Connors and M. A. Paradiso, in *Neuroscience: Exploring the Brain*, High Education Press, Beijing, 2007, pp. 761–793.
21 Z. Q. Wang, H. Y. Xu, X. H. Li, H. Yu, Y. C. Liu and X. J. Zhu, *Adv. Funct. Mater.*, 2012, **22**, 2759–2765.
22 H. Z. Shouval, S. S.-H. Wang and G. M. Wittenberg, *Front. Comput. Neurosci.*, 2010, **4**, 19.
23 L. N. Cooper and M. F. Bear, *Nat. Rev. Neurosci.*, 2012, **13**, 798–810.
24 J. Lisman and N. Spruston, *Nat. Neurosci.*, 2005, **8**, 839–841.
25 A. Mehonic, S. Cueff, M. Wojdak, S. Hudziak, C. Labbé, R. Rizk and A. J. Kenyon, *Nanotechnology*, 2012, **23**, 455201.
26 G. S. Tang, F. Zeng, C. Chen, H. Y. Liu, S. Gao, C. Song, Y. S. Lin, G. Chen and F. Pan, *Nanoscale*, 2013, **5**, 422–428.
27 W. C. Abraham, *Nat. Rev. Neurosci.*, 2008, **9**, 387–399.
28 Q. Liu, J. Sun, H. B. Lv, S. B. Long, K. B. Yin, N. Wan, Y. T. Li, L. T. Sun and M. Liu, *Adv. Mater.*, 2012, **24**, 1844–1849.
29 O. Bunău and Y. Joly, *Phys. Rev. B: Condens. Matter Mater. Phys.*, 2012, **85**, 155121.
30 H. Thakur, R. Kumar, P. Thakur, N. B. Brookes, K. K. Sharma, A. P. Singh, Y. Kumar, S. Gautam and K. H. Chae, *J. Appl. Phys.*, 2011, **110**, 083718.
31 M. E. Fleet, S. L. Harmer, X. Liu and H. W. Nesbitt, *Surf. Sci.*, 2005, **584**, 133–145.
32 X. Xu, R. A. Register and S. R. Forrest, *Appl. Phys. Lett.*, 2006, **89**, 142109.
33 P. J. Chia, L. L. Chua, S. Sivaramakrishnan, J. M. Zhuo, L. H. Zhao, W. S. Sim, Y. C. Yeo and P. K. H. Ho, *Adv. Mater.*, 2007, **19**, 4202–4207.
34 C. Chen, S. Gao, G. S. Tang, C. Song, F. Zeng and F. Pan, *IEEE Electron Device Lett.*, 2012, **33**, 1711–1713.

 This journal is © The Royal Society of Chemistry 2014